Springer

KSME

Journal of Mechanical Science and Technology 31 (4) (2017) 1773~1787
www.springerlink.com/content/1738-494x(Print)/1976-3824(Online)
DOI 10.1007/s12206-017-0325-8

Thermo-electro-mechanical buckling analysis of cylindrical nanoshell on the basis of modified couple stress theory †

Fahimeh Mehralian[1] and Yaghoub Tadi Beni[2,*]

[1]*Mechanical Engineering Department, Shahrekord University, Shahrekord, Iran*
[2]*Faculty of Engineering, Shahrekord University, Shahrekord, Iran*

(Manuscript Received February 28, 2016; Revised November 7, 2016; Accepted December 14, 2016)

Abstract

In the present study, the buckling of piezoelectric cylindrical nanoshell subjected to an axial compression, an applied voltage and uniform temperature change resting on Winkler-Pasternak foundation is studied analytically. The modified couple stress theory combined with the geometrical nonlinear shell model is employed to derive the equilibrium equations and boundary conditions. The numerical results are proposed for the buckling of simply supported cylindrical nanoshell using the Navier-type solution. Thus, the effects of different parameters such as dimensionless length scale parameter, length and thickness to radius ratio, temperature change, external electric voltage and Winkler and Pasternak foundation stiffness on critical buckling load are illustrated. It is shown that increase in dimensionless length scale parameter results in increasing critical buckling load and even intensifying the influence of other parameters, such as length and thickness, on critical buckling load.

Keywords: Modified couple stress theory; Shell model; Size effect; Thermo-electro-mechanical buckling

1. Introduction

Today, the advance of smart structures thanks the invention of piezoelectric nanostrutures due to its promising mechanical, thermal and electrical properties. ZnO piezoelectric nanowires was first reported by Pan et al. and opened a new field of research in various fields of nonamechanics and nanoelectronics [1]. The superior properties of piezoelectric nanostructures lead to its extensive usages in many nanodevices like nanoresonators, nanogenerators, light-emitting diodes, and chemical sensors [2-4]. Indeed, the coupled electro-mechanical properties of piezoelectric materials, generating electrical charge under external mechanical deformation, and reversely, deforming under electrical charge, permits them to be used as sensors and actuators [5, 6]. Therefore, due to the various practical applications and further development of piezoelectric-based nanodevices, the study of their behavior, such as their deformation under different loads, is of both theoretical significance and practical value. Hence, the buckling behavior of the piezoelectric nanostucturs has attracted the attention of many researchers. For example, the axial buckling of piezoelectric nanowires under distributed transverse loading on the basis of Timoshenko beam theory and considering surface effect was investigated by Samaei et al. and the dependency of critical electric potential of buckling on both surface stresses and piezoelectricity was shown [7]. Yan et al. studied the vibration and buckling of piezoelectric nanoplate affected the surface effects, using the modified Kirchhoff plate model and the sensitivity of the critical electric voltage of buckling to the plate thickness and aspect ratio was discussed [8]. Arani et al. studied the thermo-mechanical-torsional and axial buckling of double-walled boron nitride nanotube using the nonlocal elasticity and piezoelasticity theories on Winkler-Pasternak medium and the effects of some parameters such as nonlocal parameter, temperature change, piezoelectric and dielectric constants on the critical buckling load were shown [9, 10].

In order to examine the piezoelectric nanostructures more precisely, an appropriate approach should be used. Both theoretical and experimental approaches are utilized to investigate their behaviors. However, with regard to the difficulties of experiments at submicron size, the theoretical analysis, including atomistic simulations and continuum mechanics, are becoming more important. As the molecular dynamic simulation is complicated and time consuming for large scale systems [11, 12]; thus, these limitations inspired researchers to use the continuum based models which are computationally more efficient [13-15]. On the other hand, based on the experimental observation, the size effect in small scale structures due to impurities, crystal lattice mismatch and nano cracks plays an

*Corresponding author. Tel.: +98 38 32324438, Fax.: +98 38 32324438
E-mail address: tadi@eng.sku.ac.ir
† Recommended by Associate Editor Heung Soo Shin

important role, which cannot be ignored anymore [16-18]. Therefore, there has been considerable attentions towards the modification of generalized continuum theory which account for the size effect [19-27].

The nonlocal elasticity theory is a higher order continuum theory introduced by Eringen and accordingly many studies have been done [28, 29]. For example, Liu et al. investigated the thermo-electro-mechanical free vibration of piezoelectric nanoplates on the basis of nonlocal theory and using the Kirchhoff model [30]. The piezoelectric nanoplate was considered under the biaxial force, an external electric voltage and a uniform temperature change. The thermo-electro-mechanical vibration of piezoelectric cylindrical nanoshell was examined by Ke et al. using the nonlocal theory and Love's thin shell model and the effect of some parameters such as nonlocal parameter, temperature rise, external electric voltage were studied [31]. The influence of nonlocal parameter and thermoelectric loading was shown significant.

Another higher order continuum theory is couple stress theory which was initially introduced by Mindlin, Toupin, Koiter and contains two material length scale parameters in addition two Lame constants [32-34]. Many studies are accomplished on the basis of this theory [35, 36]. Afterwards, the modified couple stress theory which has a symmetric couple stress tensor unlike classical one and only includes one material length scale parameter was proposed by Yang et al. [37]. Using the modified couple stress theory based on the shell model Sahmani et al. investigated the size-dependent dynamic stability response of functionally graded shear deformable microshells and illustrated the effect of dimensionless length scale parameter variation on the width of the instability region [38]. Kim et al. presented the analytical solutions of a general third-order plate theory on the basis of modified couple stress theory and the effect of microstructure-dependent size parameter and power law distribution of two materials on bending, buckling and vibration were discussed [39].

Mindlin presented the general gradient elastic theory, which includes higher order strain gradients. Afterwards, in simplified version, which only has five material length scale parameters, the second-order deformation gradients are included which has an anti-symmetric part and a symmetric part [40, 41]. By modifying this formulation, the strain gradient theory has been developed by Fleck and Hutchinson [42]. And ultimately, by using the higher order equilibrium equation introduced by Yang et al., the modified strain gradient theory has been presented by Lam et al. [43]. This theory includes three material length scale parameters related to the dilation tensor, the deviatoric stretch gradient tensor and the symmetric rotation gradient tensor. Gholami et al. examined the axial buckling behavior of functionally graded circular cylindrical microshells on the basis of modified strain gradient theory and using first-order shear deformable shell model [44]. The size-dependent sinusoidal beam model using the modified strain gradient theory for analysis the buckling of microbeam was studied by Akgöz et al. [45]. The size dependency illustrated very important when the thickness of the microbeam was closer to material length scale parameter.

Since the structural element of nanotubes is more similar to the cylindrical shell, an appropriate model in view of this specification should be taken into account. Thus, in order to achieve more accurate results, the use of shell model has attracted the attention of many researchers [46-49]. Mehralian et al. developed the functionally graded cylindrical thin shell model using modified couple stress theory to investigate the torsional buckling of nanotubes [50]. Ansari et al. investigated the vibration and dynamic instability of a functionally graded microshell conveying fluid on the basis of modified couple stress theory and discussed the effect of different parameters such as fluid velocity, length scale parameter and gradient index on natural frequency [51]. Tadi Beni et al. examined the free vibration of functionally graded cylindrical nanoshell based on the modified couple stress theory and first order shear deformable shell model and illustrated considerable effect of size parameter on natural frequency [52]. The three dimensional theory of elasticity was utilized by Alibeigloo et al. to investigate the vibration of SWCNT using the nonlocal theory and the effect of size parameter on natural frequency was discussed [53]. Zeverdejani et al. using thin cylindrical shell model based on the modified couple stress theory investigated the vibration of protein microtubules and illustrated the effects of some parameters like MT dimensions and size parameters on the axial and circumferential vibration frequency [54].

Since piezoelectric materials, as smart materials, have found a wide range of applications in many nanostructures, buckling analysis of piezoelectric cylindrical nanoshells subjected to the simultaneous mechanical, thermal and electrical loadings is of primary importance in the design of smart nanodevices. Moreover, due to the difficulties of nanoscale experiments and time consuming of atomistic simulation, the higher order continuum theories, as a good alternative and efficient method, have been developed to analysis bending, buckling and vibration of nanostructures. As such, there are several researches in the field of thermal investigation in conjunction with electro-mechanical analysis of nanoshells [9, 10]. The bending stability of CNTs subjected to thermo-electro-mechanical loadings was investigated by Yao et al. and the effect of temperature and electric changes on the buckling bending moment was illustrated as well; such that, the buckling bending moment increases by increase in temperature change at room or lower temperature and decreases by increase in temperature change at higher temperature [78]. Yao et al. studied the torsional buckling behavior of CNTs with considering small scale effect under thermo-electro-mechanical loadings and investigated the influence of different parameters on the critical buckling torque as well [79]. Besides shell element, beam and plate elements were studied under thermo-electro-mechanical loadings by Ebrahimi et al. and the effects of different parameters on the critical buckling load were shown at the meantime [75, 80].

Motivated by this considerations, this paper for the first

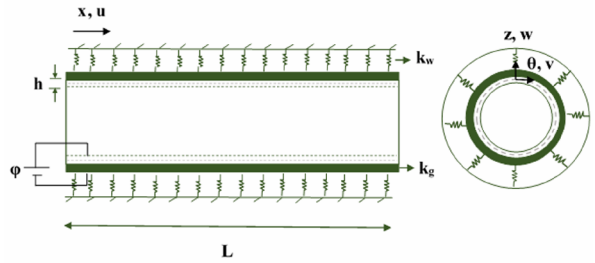

Fig. 1. Configuration of the cylindrical shell.

time investigates the thermo-electro-mechanical buckling of piezoelectric cylindrical nanoshells based on the modified couple stress theory. The formulation is developed on the basis of modified couple stress theory with regard to the geometric nonlinearity. The governing equations and boundary conditions are derived using the potential energy principle.

Thus, the formulation derived here have following novelties, benefits and characteristics simultaneously:

First, the formulation derived here for studying the thermo-electro-mechanical buckling of cylindrical nanoshell can be reduced to only one loading condition.

Second, this formulation is able to predict the behavior of shell structures more realistically due to using the cylindrical shell model.

Third, the size effect is considered in this formulation through using the modified couple stress theory and this formulation can turn into the classical shell formulation as well.

Also, as a case study, the buckling behavior of simply supported cylindrical nanoshell, are investigated. The effect of different parameters such as material length scale parameter, thickness ratio, length ratio and Winkler and Pasternak foundation stiffness parameter on the critical buckling load is illustrated.

2. Preliminary

Consider a cylindrical nanoshell resting on the Winkler-Pasternak elastic foundation subjected to a uniform distributed axial compressive load, uniform temperature change and an applied electric voltage $\varphi(x,\theta,z)$ as shown in Fig. 1. The origin of the coordinate system is located in the middle surface of nanoshell which x and θ axis are the longitudinal and circumferential direction and z axis normal to them and toward outside. The length, radius and thickness of thin cylindrical shell are L, R and h, respectively.

2.1 Modified couple stress theory

Based on the modified couple stress theory, the strain energy in a continuum made of a linear elastic material occupying a volume Ω and is subjected to infinitesimal deformation can be derived as [37]:

$$\tilde{U}_s = \frac{1}{2}\int_\Omega \left(\sigma_{ij}\varepsilon_{ij} + m_{ij}\chi_{ij} - D_i E_i\right) dV \tag{1}$$

where σ_{ij}, D_i and m_{ij} are the components of the Cauchy stress tensor, electric displacement vector and the higher order stress tensor and ε_{ij}, E_i and χ_{ij} are the components of strain tensor, electric field vector and the symmetric part of rotation gradient tensor respectively and obtained as:

$$\sigma_{ij} = c_{ijkl}\varepsilon_{kl} - e_{mij}\mathrm{E}_m - \beta_{ij}\Delta T \tag{2}$$

$$D_i = e_{ikl}\varepsilon_{kl} + s_{im}\mathrm{E}_m + p_i\Delta T \tag{3}$$

$$m_{ij} = 2l^2 c_{66}\chi_{ij} \tag{4}$$

$$\varepsilon_{ij} = \frac{1}{2}\left(u_{i,j} + u_{j,i} + u_{3,i}u_{3,j}\right) \tag{5}$$

$$E_i = -\phi_{,i} \tag{6}$$

$$\chi_{ij} = \frac{1}{4}\left(e_{ipq}\eta_{jpq} + e_{jpq}\eta_{ipq}\right) \tag{7}$$

in which c_{ijkl}, e_{mij}, s_{im}, β_{ij} and p_i are the components of elastic tensor, piezoelectric constants, dielectric constants, thermal moduli and pyroelectric constants, respectively and u_i, φ, ΔT, e_{ipq} and η_{ipq} represent the components of displacement vector, electric potential, temperature change, Permutation symbol and deviatoric stretch gradient tensor, respectively. l indicates the material length scale parameter related to the symmetric rotation gradient.

Hence, the constitutive equation for piezoelectric cylindrical shell under the plane stress state is given by:

$$\begin{Bmatrix}\sigma_{xx}\\ \sigma_{\theta\theta}\\ \sigma_{x\theta}\end{Bmatrix} = \begin{bmatrix}\tilde{c}_{11} & \tilde{c}_{12} & 0\\ \tilde{c}_{12} & \tilde{c}_{11} & 0\\ 0 & 0 & \tilde{c}_{66}\end{bmatrix}\begin{Bmatrix}\varepsilon_{xx}\\ \varepsilon_{\theta\theta}\\ \gamma_{x\theta}\end{Bmatrix} - \begin{bmatrix}0 & 0 & \tilde{e}_{13}\\ 0 & 0 & \tilde{e}_{13}\\ 0 & 0 & 0\end{bmatrix}\begin{Bmatrix}E_x\\ E_\theta\\ E_z\end{Bmatrix} - \begin{bmatrix}\tilde{\beta}_1\\ \tilde{\beta}_1\\ 0\end{bmatrix}\Delta T \tag{8}$$

$$\begin{Bmatrix}D_x\\ D_\theta\\ D_z\end{Bmatrix} = \begin{bmatrix}0 & 0 & 0\\ 0 & 0 & 0\\ \tilde{e}_{13} & \tilde{e}_{13} & 0\end{bmatrix}\begin{Bmatrix}\varepsilon_{xx}\\ \varepsilon_{\theta\theta}\\ \gamma_{x\theta}\end{Bmatrix} + \begin{bmatrix}\tilde{s}_{11} & 0 & 0\\ 0 & \tilde{s}_{11} & 0\\ 0 & 0 & \tilde{s}_{33}\end{bmatrix}\begin{Bmatrix}E_x\\ E_\theta\\ E_z\end{Bmatrix} + \begin{bmatrix}\tilde{p}_1\\ \tilde{p}_1\\ \tilde{p}_3\end{bmatrix}\Delta T \tag{9}$$

where $\tilde{c}_{ij}$, $\tilde{e}_{ij}$, $\tilde{s}_{ij}$, $\tilde{\beta}_i$ and $\tilde{p}_i$ are respectively the reduced elastic, piezoelectric, dielectric constants and thermal moduli and pyroelectric constants for the piezoelectric shell and defined as [30, 31]:

$$\begin{aligned}&\tilde{c}_{11} = c_{11} - \frac{c_{13}^2}{c_{33}},\ \tilde{c}_{12} = c_{12} - \frac{c_{13}^2}{c_{33}},\ \tilde{c}_{66} = c_{66},\\ &\tilde{e}_{31} = e_{31} - \frac{c_{13}e_{33}}{c_{33}},\ \tilde{s}_{11} = s_{11},\ \tilde{s}_{33} = s_{33} - \frac{e_{33}^2}{c_{33}},\\ &\tilde{\beta}_1 = \beta_1 - \frac{c_{13}\beta_3}{c_{33}},\ \tilde{p}_1 = p_1,\ \tilde{p}_3 = p_3 + \frac{e_{33}\beta_3}{c_{33}}.\end{aligned} \tag{10}$$

According to Refs. [31, 55], the electric potential is considered to change as a combination of a cosine and linear variation, satisfied the Maxwell equation, as below:

$$\phi(x,\theta,z) = -\cos(\beta z)\varphi(x,\theta) + \frac{2zV_0}{h} \tag{11}$$

in which, $\beta = \pi/h$; $\varphi(x,\theta)$ and V_0 represent the spatial variation of the electric potential in the mid-plane and the external electric voltage, respectively.

Experiments reveal an increase in materials characteristics with decreasing the size at the ultra-small scales. All these experiments imply that when the characteristic size (thickness, diameter, etc.) of a micro/nano element is in the order of its intrinsic the material length scales (typically sub-micron), the material elastic constants highly depend on the element dimensions. Unfortunately, while much is known about the mechanical characteristics of isolated bulk materials, the properties of material at nanoscale cannot necessarily be predicted from those measured at larger scales. The source of difference between the mechanical properties of ultra-small and bulk materials with the same composition can be attributed to several physical phenomena such as differences in structure, deformation, or fracture mechanisms. The differences typically occur when the material dimensions reach characteristic length scales that are associated with defect dimensions such as dislocation, spacing and grain size. At nanoscale level, the gradient deformations vary sharply, hence the microscopic stresses and strains are not constant and depend on the shrinking length scale of the nanostructures: The smaller the structure, the more rapid the microscopic fields vary, and they do so in a way that leads to either stiffening or softening of the material. In order to model these gradient effects, a higher order continuum theory i.e. couple stress theory was introduced with length scale parameters. A length scale parameter might be considered as a mathematical parameter that scales the strain gradients in the constitutive model so as to balance the dimensions of strains and strain gradients. As the characteristic length of the deformation field becomes significantly larger than the material length scale parameter, strain gradient effects become negligible because the strain terms are much larger than their scaled gradient terms. In this case, the results obtain via modified couple stress theory is the same as that of classical theory. Note that classical continuum mechanics is unable to simulate the size effect in micro/nano structures. Also, it is still not possible to conduct time-consuming molecular simulations on realistic structures.

It should be noted that since the higher-order electromechanical coupling, induced by the strain gradient, is neglected then the piezoelectric properties do not consider size dependent. This assumption, neglecting the higher-order electromechanical induced by the strain gradient, is utilized in many nano-scale studied and consequently there are many studied in which the electric potential distribution is considered similar to Eq. (11) [30, 31, 63-75].

2.2 Displacement and electric field of cylindrical shell

The displacement field according to Love's thin shell theory is indicated by u, v and w along the three directions x, θ and z and can be written as [56]:

$$\begin{aligned} u(x,\theta,z) &= U(x,\theta) - z\frac{\partial W(x,\theta)}{\partial x} \\ v(x,\theta,z) &= V(x,\theta) - \frac{z}{R}\left(\frac{\partial W(x,\theta)}{\partial \theta} - V(x,\theta)\right) \\ w(x,\theta,z) &= W(x,\theta) \end{aligned} \tag{12}$$

where $U(x, \theta)$, $V(x, \theta)$ and $W(x, \theta)$ are the middle surface displacements. The electric field according to Eq. (6), can be obtained as follows [57]:

$$\begin{aligned} E_x &= -\frac{\partial \phi}{\partial x} = \cos(\beta z)\frac{\partial \varphi}{\partial x} \\ E_\theta &= -\frac{1}{R}\frac{\partial \phi}{\partial \theta} = \frac{\cos(\beta z)}{R}\frac{\partial \varphi}{\partial \theta} \\ E_z &= -\frac{\partial \phi}{\partial z} = -\beta \sin(\beta z)\varphi - \frac{2V_0}{h}. \end{aligned} \tag{13}$$

3. Governing equations and boundary conditions

Based on the previous section, in order to obtain the equilibrium equations and boundary conditions using the modified couple stress theory, the principle of minimum potential energy and calculus of variation method, take the following steps:

- First, calculate the classical and non-classical strain tensors by using displacement field and utilizing Eqs. (5) and (7), according to Ref. [50].
- Second, calculate the Cauchy, higher order stress tensor and electric displacement vector's components by substituting the strain and symmetric part of rotation gradient tensor besides electric field into the constitutive Eqs. (4), (8) and (9).
- Third, determine the strain energy by substituting the classical and non-classical stresses as well as classical and non-classical strains besides electric field and electric displacement in Eq. (1).
- Fourth, derive the equilibrium equations and boundary conditions by substituting strain energy and work of external forces into the principle of minimum potential energy and using calculus of variations.

Therefore, the strain and symmetric rotation gradient tensor' components are obtained as:

$$\begin{aligned} \varepsilon_{xx} &= \frac{\partial U}{\partial x} + \frac{1}{2}\left(\frac{\partial W}{\partial x}\right)^2 - z\frac{\partial^2 W}{\partial x^2} \\ \varepsilon_{\theta\theta} &= \frac{1}{R}\left(\frac{\partial V}{\partial \theta} + W + \frac{1}{2R}\left(\frac{\partial W}{\partial \theta}\right)^2 - \frac{z}{R}\frac{\partial^2 W}{\partial \theta^2}\right) \\ \varepsilon_{x\theta} &= \varepsilon_{\theta x} = \frac{1}{2}\left(\frac{1}{R}\frac{\partial U}{\partial \theta} + \frac{\partial V}{\partial x} + \frac{1}{R}\frac{\partial W}{\partial x}\frac{\partial W}{\partial \theta} - \frac{2z}{R}\frac{\partial^2 W}{\partial x \partial \theta}\right). \end{aligned} \tag{14}$$

It should be noted that the numerical results has illustrated

that the rotations including U and V are of insignificant effect for shells whose displacement components are rapidly varying functions of shell coordinate [58]. Thus, these terms are neglected in strain components.

Moreover, the non-classical strain components are obtained as:

$$\chi_{zz}=\frac{1}{2R^2}\left(\frac{\partial U}{\partial\theta}-2z\frac{\partial^2 W}{\partial x\partial\theta}+R\frac{\partial V}{\partial x}\right) \tag{15}$$

$$\chi_{xx}=\frac{1}{R}\left(\frac{\partial^2 W}{\partial x\partial\theta}-\frac{\partial V}{\partial x}\right)$$

$$\chi_{\theta\theta}=\frac{1}{2R}\left(\frac{\partial V}{\partial x}-\frac{1}{R}\frac{\partial U}{\partial\theta}-2\frac{\partial^2 W}{\partial x\partial\theta}\right)$$

$$\chi_{x\theta}=\chi_{\theta x}=\frac{1}{2}\left(\frac{1}{R^2}\left(\frac{\partial^2 W}{\partial\theta^2}-\frac{\partial V}{\partial\theta}\right)-\frac{\partial^2 W}{\partial x^2}\right)$$

$$\chi_{z\theta}=\chi_{\theta z}=\frac{1}{4R}\left(\frac{\partial^2 V}{\partial x\partial\theta}-\frac{1}{R}\frac{\partial^2 U}{\partial\theta^2}+2\frac{\partial W}{\partial x}-\frac{z^2}{R^2}\frac{\partial^3 W}{\partial x\partial\theta^2}\right)$$

$$\chi_{xz}=\chi_{zx}=\frac{1}{4}\left(\frac{\partial^2 V}{\partial x^2}-\frac{1}{R}\frac{\partial^2 U}{\partial x\partial\theta}-\frac{z^2}{R^2}\frac{\partial^3 W}{\partial x^2\partial\theta}\right).$$

Afterwards, in order to obtain the strain energy, the Cauchy, higher order stress tensors and electric displacement vector should be derived by using the classical and non-classical strains and electric field.

In order to achieve the equilibrium equations and boundary conditions, the principle of minimum potential energy is utilized as:

$$\delta\Pi=\delta\tilde{U}_s-\delta\tilde{W}=0 \tag{16}$$

where $\delta\tilde{U}_s$ represents for strain energy variation, and $\delta\tilde{W}$ is the variation of the work of external forces acting on the cylindrical shell.

Also, by substituting classical and non-classical strains and stresses and electric field and displacement into the modified couple stress theory relation, the strain energy is obtained as follows:

$$\delta\tilde{U}_s=\int_{\Omega}\left(\sigma_{ij}\delta\varepsilon_{ij}+m_{ij}\delta\chi_{ij}-D_i\delta E_i\right)dV=\int_\theta\int_x\Bigg[N_{xx}\left(\frac{\partial\delta U}{\partial x}+\frac{\partial W}{\partial x}\frac{\partial\delta W}{\partial x}\right)-M_{xx}\left(\frac{\partial^2\delta W}{\partial x^2}\right)+N_{\theta\theta}\left(\frac{1}{R}\left(\frac{\partial\delta V}{\partial\theta}+\delta W\right)+\frac{1}{R^2}\frac{\partial W}{\partial\theta}\frac{\partial\delta W}{\partial\theta}\right)-M_{\theta\theta}\frac{1}{R^2}\left(\frac{\partial^2\delta W}{\partial\theta^2}\right)+N_{x\theta}\left(\frac{1}{R}\frac{\partial\delta U}{\partial\theta}+\frac{\partial\delta V}{\partial x}+\frac{1}{R}\frac{\partial\delta W}{\partial x}\frac{\partial W}{\partial\theta}+\frac{1}{R}\frac{\partial W}{\partial x}\frac{\partial\delta W}{\partial\theta}\right)-M_{x\theta}\left(\frac{2}{R}\left(\frac{\partial^2\delta W}{\partial x\partial\theta}\right)\right)+Y_{zz}\left(\frac{1}{2R^2}\left(\frac{\partial\delta U}{\partial\theta}+R\frac{\partial\delta V}{\partial x}\right)\right)-T_{zz}\left(\frac{1}{R^2}\frac{\partial^2\delta W}{\partial x\partial\theta}\right)$$

$$+Y_{xx}\left(\frac{1}{R}\left(\frac{\partial^2\delta W}{\partial x\partial\theta}-\frac{\partial\delta V}{\partial x}\right)\right)+Y_{\theta\theta}\left(\frac{1}{2R}\left(\frac{\partial\delta V}{\partial x}-\frac{1}{R}\frac{\partial\delta U}{\partial\theta}-2\frac{\partial^2\delta W}{\partial x\partial\theta}\right)\right)+Y_{x\theta}\left(\left(\frac{1}{R^2}\left(\frac{\partial^2\delta W}{\partial\theta^2}-\frac{\partial\delta V}{\partial\theta}\right)-\frac{\partial^2\delta W}{\partial x^2}\right)\right)+Y_{z\theta}\left(\frac{1}{2R}\left(\frac{\partial^2\delta V}{\partial x\partial\theta}-\frac{1}{R}\frac{\partial^2\delta U}{\partial\theta^2}+2\frac{\partial\delta W}{\partial x}\right)\right)+Y_{zx}\left(\frac{1}{2}\left(\frac{\partial^2\delta V}{\partial x^2}-\frac{1}{R}\frac{\partial^2\delta U}{\partial x\partial\theta}\right)\right)-\int_{-h/2}^{h/2}\left(D_x\cos(\beta z)\frac{\partial\delta\varphi}{\partial x}+D_\theta\frac{\cos(\beta z)}{R}\frac{\partial\delta\varphi}{\partial\theta}-D_z\beta\sin\beta z\delta\varphi\right)dz\Bigg]Rdxd\theta\,. \tag{17}$$

In addition, the in-plane force and moment resultants in Eq. (17), are defined as:

$$N_{ij}=\int_{-h/2}^{-h/2}\sigma_{ij}dz,\qquad M_{ij}=\int_{-h/2}^{-h/2}\sigma_{ij}zdz \tag{18}$$

$$Y_{ij}=\int_{-h/2}^{h/2}m_{ij}dz,\qquad T_{ij}=\int_{-h/2}^{h/2}m_{ij}zdz\,. \tag{19}$$

Since the cylindrical shell is resting on the Winkler-Pasternak elastic medium, the variation of work done on nanoshell is determined as below:

$$\delta\tilde{W}=\delta\tilde{W}_f+\delta\tilde{W}_{ef} \tag{20}$$

$$\delta\tilde{W}_f=\int_\theta\frac{P}{2\pi R}\delta U\Big|_{x=0,L}Rd\theta$$

$$\delta\tilde{W}_{ef}=\int_x\int_\theta\left(-k_wW+k_g\nabla^2W\right)\delta W\,Rd\theta dx$$

$$\nabla^2=\frac{\partial^2}{\partial x^2}+\frac{1}{R^2}\frac{\partial^2}{\partial\theta^2}$$

where P is external axial compression load, k_w is the Winkler foundation stiffness and k_g is the shear subgrade modulus of the foundation. Thus, by substituting Eqs. (17) and (20) in Eq. (16) and taking the variation and performing integrating by parts, the equilibrium equations are derived as:

$$A_1\frac{\partial^2U}{\partial x^2}+A_2\frac{\partial^4U}{\partial x^2\partial\theta^2}+A_3\frac{\partial^4V}{\partial x^3\partial\theta}+A_4\frac{\partial^2V}{\partial x\partial\theta}+A_5\frac{\partial^4V}{\partial x\partial\theta^3}+A_6\frac{\partial W}{\partial x}+A_7\frac{\partial^3W}{\partial x\partial\theta^2}+A_8\frac{\partial^2U}{\partial\theta^2}+A_9\frac{\partial^4U}{\partial\theta^4}=0 \tag{21}$$

$$B_1\frac{\partial^4V}{\partial x^4}+B_2\frac{\partial^2V}{\partial x^2}+B_3\frac{\partial^2V}{\partial\theta^2}+B_4\frac{\partial^4V}{\partial x^2\partial\theta^2}+B_5\frac{\partial^4U}{\partial x^3\partial\theta}+B_6\frac{\partial^4U}{\partial x\partial\theta^3}+B_7\frac{\partial^2U}{\partial x\partial\theta}+B_8\frac{\partial^3W}{\partial x^2\partial\theta}+B_9\frac{\partial^3W}{\partial\theta^3}+B_{10}\frac{\partial W}{\partial\theta}=0 \tag{22}$$

$$C_1\frac{\partial^4W}{\partial x^4}+C_2\frac{\partial^2W}{\partial x^2}+C_3\frac{\partial^4W}{\partial x^2\partial\theta^2}+C_4\frac{\partial U}{\partial x}+C_5\frac{\partial^3U}{\partial x\partial\theta^2}+C_6\frac{\partial^3V}{\partial x^2\partial\theta}+C_7\frac{\partial V}{\partial\theta}+C_8\frac{\partial^3V}{\partial\theta^3}+C_9W+C_{10}\frac{\partial^4W}{\partial\theta^4} \tag{23}$$

$$+C_{11}\frac{\partial^2\varphi}{\partial x^2}+C_{12}\frac{\partial^2\varphi}{\partial\theta^2}+C_{13}-\left(N_{xx}\frac{\partial^2W}{\partial x^2}+\frac{2}{R}N_{x\theta}\frac{\partial^2W}{\partial x\partial\theta}\right.$$
$$\left.+\frac{1}{R^2}N_{\theta\theta}\frac{\partial^2W}{\partial\theta^2}\right)+k_wW-k_g\left(\frac{\partial^2W}{\partial x^2}+\frac{1}{R^2}\frac{\partial^2W}{\partial\theta^2}\right)=0$$
$$D_1\frac{\partial^2\varphi}{\partial x^2}+D_2\frac{\partial^2\varphi}{\partial\theta^2}+D_3\frac{\partial^2W}{\partial x^2}+D_4\frac{\partial^2W}{\partial\theta^2}+D_5\varphi=0 \tag{24}$$

where due to the combination of thermo-mechanical loadings, we have:

$$N_{xx}=N_{xx}^M+N_{xx}^T+N_{xx}^E \tag{25}$$
$$N_{\theta\theta}=N_{\theta\theta}^T+N_{\theta\theta}^E$$

which superscript M ,T and E refer to mechanical, thermal and electrical component of loads. Moreover, according to Hook's law and linear membrane equilibrium equations, the mechanical prebuckling resultant force in θ direction is neglected.

Boundary conditions of the cylindrical shell on the θ edge haven't been written, due to the variation of θ from 0 to 2π and only boundary conditions on the longitudinal edges are considered; thus, the boundary conditions on the x edge are as follows:

$$\int_\theta\left[a_1\frac{\partial U}{\partial x}+a_2\frac{\partial^3U}{\partial x\partial\theta^2}+a_3\frac{\partial^3V}{\partial x^2\partial\theta}+a_4\frac{\partial V}{\partial\theta}+a_5W\right.$$
$$\left.a_6\right]d\theta\Big|_{x=0,L}=0\ \text{ or }\ \delta U\Big|_{x=0,L}=0 \tag{26}$$

$$\int_\theta\left[b_1\frac{\partial^3V}{\partial x^3}+b_2\frac{\partial V}{\partial x}+b_3\frac{\partial^3V}{\partial x\partial\theta^2}+b_4\frac{\partial^3U}{\partial x^2\partial\theta}+b_5\frac{\partial^3U}{\partial\theta^3}\right.$$
$$\left.+b_6\frac{\partial U}{\partial\theta}+b_7\frac{\partial^2W}{\partial x\partial\theta}\right]d\theta\Big|_{x=0,L}=0\ \text{ or }\ \delta V\Big|_{x=0,L}=0 \tag{27}$$

$$\int_\theta\left[b_8\frac{\partial^2U}{\partial x\partial\theta}+b_9\frac{\partial^2V}{\partial x^2}\right]d\theta\Big|_{x=0,L}=0$$
$$\text{or}\ \ \delta\left(\frac{\partial V}{\partial x}\right)\Big|_{x=0,L}=0 \tag{28}$$

$$\int_\theta\left[c_1\frac{\partial^3W}{\partial x^3}+c_2\frac{\partial W}{\partial x}+c_3\frac{\partial^3W}{\partial x\partial\theta^2}+c_4\frac{\partial^2U}{\partial\theta^2}+c_5\frac{\partial^2V}{\partial x\partial\theta}\right.$$
$$\left.+c_6\frac{\partial\varphi}{\partial x}+\left(N_{xx}^M+N_{xx}^T+N_{xx}^E\right)\frac{\partial W}{\partial x}\right]d\theta\Big|_{x=0,L}=0 \tag{29}$$
$$\text{or}\ \ \delta W\Big|_{x=0,L}=0$$

$$\int_\theta\left[c_7\frac{\partial^2W}{\partial x^2}+c_8\frac{\partial^2W}{\partial\theta^2}+c_9\frac{\partial V}{\partial\theta}+c_{10}\varphi\right]d\theta\Big|_{x=0,L}=0$$
$$or\ \ \delta\left(\frac{\partial W}{\partial x}\right)\Big|_{x=0,L}=0 \tag{30}$$

$$\int_\theta\int_{-h/2}^{h/2}\left[-D_x\cos(\beta z)\right]dzd\theta\Big|_{x=0,L}=0\ \ or\ \ \delta\varphi\Big|_{x=0,L}=0\,. \tag{31}$$

The coefficients A_1 to A_9, B_1 to B_{10} and C_1 to C_{13} and a_1 to a_6, b_1 to b_9 and c_1 to c_{10} in the above equations are written in Appendix A.1.

4. Solution procedure

Utilizing the adjacent equilibrium criterion, the stability equations of circular cylindrical shell are obtained. The small increments to the displacement variables have been given in order to investigate the possible existence of adjacent-equilibrium configurations. Afterwards, the two adjacent configurations indicated by displacements before and after increment are investigated. Thus:

$$U=U_0+U_1 \tag{32}$$
$$V=V_0+V_1$$
$$W=W_0+W_1$$

where U_0, V_0 and W_0 are displacement components of the equilibrium state and U_1, V_1 and W_1 are arbitrary small increment. Thus, (U_0, V_0 and W_0) and (U, V and W) are adjacent equilibrium configurations related to a single value of applied load. Similar to Eq. (32), the electric potential are found to be the sum of those related to the equilibrium and neighboring states as:

$$\varphi=\varphi_0+\varphi_1\,. \tag{33}$$

By substituting Eqs. (32) and (33) into equilibrium equations (Eqs. (21)-(24)), all terms alone in U_0, V_0, W_0 and φ_0 drop out because U_0, V_0, W_0 and φ_0 are a solution of equilibrium equations. Besides, quadratic and higher order terms in U_1, V_1 and W_1 are neglected due to their smallness; therefore, the resulting stability equations and boundary conditions are:

$$A_1\frac{\partial^2U_1}{\partial x^2}+A_2\frac{\partial^4U_1}{\partial x^2\partial\theta^2}+A_3\frac{\partial^4V_1}{\partial x^3\partial\theta}+A_4\frac{\partial^2V_1}{\partial x\partial\theta}+A_5\frac{\partial^4V_1}{\partial x\partial\theta^3}$$
$$+A_6\frac{\partial W_1}{\partial x}+A_7\frac{\partial^3W_1}{\partial x\partial\theta^2}+A_8\frac{\partial^2U_1}{\partial\theta^2}+A_9\frac{\partial^4U_1}{\partial\theta^4}=0 \tag{34}$$

$$B_1\frac{\partial^4V_1}{\partial x^4}+B_2\frac{\partial^2V_1}{\partial x^2}+B_3\frac{\partial^2V_1}{\partial\theta^2}+B_4\frac{\partial^4V_1}{\partial x^2\partial\theta^2}+B_5\frac{\partial^4U_1}{\partial x^3\partial\theta}$$
$$+B_6\frac{\partial^4U_1}{\partial x\partial\theta^3}+B_7\frac{\partial^2U_1}{\partial x\partial\theta}+B_8\frac{\partial^3W_1}{\partial x^2\partial\theta}+B_9\frac{\partial^3W_1}{\partial\theta^3}+B_{10}\frac{\partial W_1}{\partial\theta}=0 \tag{35}$$

$$C_1\frac{\partial^4W_1}{\partial x^4}+C_2\frac{\partial^2W_1}{\partial x^2}+C_3\frac{\partial^4W_1}{\partial x^2\partial\theta^2}+C_4\frac{\partial U_1}{\partial x}+C_5\frac{\partial^3U_1}{\partial x\partial\theta^2}$$
$$+C_6\frac{\partial^3V_1}{\partial x^2\partial\theta}+C_7\frac{\partial V_1}{\partial\theta}+C_8\frac{\partial^3V_1}{\partial\theta^3}+C_9W_1+C_{10}\frac{\partial^4W_1}{\partial\theta^4}$$
$$+C_{11}\frac{\partial^2\varphi_1}{\partial x^2}+C_{12}\frac{\partial^2\varphi_1}{\partial\theta^2}-\left(N_{xx0}\frac{\partial^2W_1}{\partial x^2}+\frac{2}{R}N_{x\theta0}\frac{\partial^2W_1}{\partial x\partial\theta}\right. \tag{36}$$
$$\left.+\frac{1}{R^2}N_{\theta\theta0}\frac{\partial^2W_1}{\partial\theta^2}\right)+k_wW_1-k_g\left(\frac{\partial^2W_1}{\partial x^2}+\frac{1}{R^2}\frac{\partial^2W_1}{\partial\theta^2}\right)=0$$

$$D_1\frac{\partial^2\varphi_1}{\partial x^2}+D_2\frac{\partial^2\varphi_1}{\partial\theta^2}+D_3\frac{\partial^2W_1}{\partial x^2}+D_4\frac{\partial^2W_1}{\partial\theta^2}+D_5\varphi_1=0 \tag{37}$$

and

$$\int_\theta \left[a_1 \frac{\partial U_1}{\partial x} + a_2 \frac{\partial^3 U_1}{\partial x \partial \theta^2} + a_3 \frac{\partial^3 V_1}{\partial x^2 \partial \theta} + a_4 \frac{\partial V_1}{\partial \theta} + a_5 W_1 \right] d\theta \Big|_{x=0,L} = 0 \quad \text{or} \quad \delta U_1 \big|_{x=0,L} = 0 \tag{38}$$

$$\int_\theta \left[b_1 \frac{\partial^3 V_1}{\partial x^3} + b_2 \frac{\partial V_1}{\partial x} + b_3 \frac{\partial^3 V_1}{\partial x \partial \theta^2} + b_4 \frac{\partial^3 U_1}{\partial x^2 \partial \theta} + b_5 \frac{\partial^3 U_1}{\partial \theta^3} + b_6 \frac{\partial U_1}{\partial \theta} + b_7 \frac{\partial^2 W_1}{\partial x \partial \theta} \right] d\theta \Big|_{x=0,L} = 0 \quad \text{or} \quad \delta V_1 \big|_{x=0,L} = 0 \tag{39}$$

$$\int_\theta \left[b_8 \frac{\partial^2 U_1}{\partial x \partial \theta} + b_9 \frac{\partial^2 V_1}{\partial x^2} \right] d\theta \Big|_{x=0,L} = 0 \quad \text{or} \quad \delta \left(\frac{\partial V_1}{\partial x} \right) \Big|_{x=0,L} = 0 \tag{40}$$

$$\int_\theta \left[c_1 \frac{\partial^3 W_1}{\partial x^3} + c_2 \frac{\partial W_1}{\partial x} + c_3 \frac{\partial^3 W_1}{\partial x \partial \theta^2} + c_4 \frac{\partial^2 U_1}{\partial \theta^2} + c_5 \frac{\partial^2 V_1}{\partial x \partial \theta} + c_6 \frac{\partial \varphi_1}{\partial x} + \left(N_{xx0}^M + N_{xx0}^T + N_{xx0}^E \right) \frac{\partial W_1}{\partial x} \right] d\theta \Big|_{x=0,L} = 0 \quad \text{or} \quad \delta W_1 \big|_{x=0,L} = 0 \tag{41}$$

$$\int_\theta \left[c_7 \frac{\partial^2 W_1}{\partial x^2} + c_8 \frac{\partial^2 W_1}{\partial \theta^2} + c_9 \frac{\partial V_1}{\partial \theta} + c_{10} \varphi_1 \right] d\theta \Big|_{x=0,L} = 0 \quad \text{or} \quad \delta \left(\frac{\partial W_1}{\partial x} \right) \Big|_{x=0,L} = 0 \tag{42}$$

$$\int_\theta \int_{-h/2}^{h/2} \left[\mathrm{d}_1 \frac{\partial \varphi_1}{\partial x} \right] dz d\theta \big|_{x=0,L} = 0 \quad \text{or} \quad \delta \varphi_1 \big|_{x=0,L} = 0 . \tag{43}$$

It should be noted that, since the influence of prebuckling rotations is negligibly small in many instances, consequently we neglect the influence of prebuckling rotations according to Ref. [58]. This approximation, is utilized by researchers in literature, like Ref. [81].

In addition, the displacement U_0, V_0 and W_0 is usually called prebucking deformation and U_1, V_1 and W_1 is called the buckling mode [58].

4.1 Buckling analysis

Consider a piezoelectric cylindrical nanoshell with simply supported edge with electric potential equal to zero at all edges of nanoshell; thus, the boundary conditions are expressed as follows:

$$\left[a_1 \frac{\partial U_1}{\partial x} + a_2 \frac{\partial^3 U_1}{\partial x \partial \theta^2} + a_3 \frac{\partial^3 V_1}{\partial x^2 \partial \theta} + a_4 \frac{\partial V_1}{\partial \theta} + a_5 W_1 \right]_{x=0,L} = 0 \tag{44}$$

$$V_1 \big|_{x=0,L} = 0 \tag{45}$$

$$\left[b_8 \frac{\partial^2 U_1}{\partial x \partial \theta} + b_9 \frac{\partial^2 V_1}{\partial x^2} \right]_{x=0,L} = 0 \tag{46}$$

$$W_1 \big|_{x=0,L} = 0 \tag{47}$$

$$\left[c_7 \frac{\partial^2 W_1}{\partial x^2} + c_8 \frac{\partial^2 W_1}{\partial \theta^2} + c_9 \frac{\partial V_1}{\partial \theta} + c_{10} \varphi_1 \right]_{x=0,L} = 0 \tag{48}$$

$$\varphi_1 \big|_{x=0,L} = 0. \tag{49}$$

The circular cylindrical shell is subjected to a uniformly distributed axial compressive load P. It should be noted that the narrow boundary zones near to the shell ends are affected by the bending of shell walls. Therefore, for simplicity, this effect of localized bending is frequently neglected and the force resultants in prebuckling state are derived considering the membrane analysis of the unbuckled cylindrical form and thermal and electrical component of load [58, 60]:

$$\begin{aligned} N_{xx0} &= N_{xx0}^M + N_{xx0}^T + N_{xx0}^E = -\frac{P}{2\pi R} - \tilde{\beta}_1 \Delta T h + 2\tilde{e}_{31} V_0 \\ N_{\theta\theta 0} &= N_{\theta\theta 0}^T = -\tilde{\beta}_1 \Delta T h + 2\tilde{e}_{31} V_0 \\ N_{x\theta 0} &= 0 \end{aligned} \tag{50}$$

however, according to Eq. (50), in circumferential direction, only thermal and electric load is taken into account.

In order to investigate the nanoshell's buckling, with consideration of the boundary conditions according to Eqs. (44)-(49), the approximate solutions may be considered as harmonic trigonometric functions, according to Refs. [31, 66, 82], as follows:

$$\begin{aligned} U_1(x,\theta) &= U_1 \cos\left(\frac{m\pi}{L} x \right) \cos(n\theta) \\ V_1(x,\theta) &= V_1 \sin\left(\frac{m\pi}{L} x \right) \sin(n\theta) \\ W_1(x,\theta) &= W_1 \sin\left(\frac{m\pi}{L} x \right) \cos(n\theta) \\ \varphi_1(x,\theta) &= \varphi_1 \sin\left(\frac{m\pi}{L} x \right) \cos(n\theta) \end{aligned} \tag{51}$$

in which U_1, V_1, W_1 and φ_1 represent constant coefficients, and *m, n* are axial and circumferential wave numbers respectively.

Thus, by substituting approximate solutions Eq. (51) into equilibrium equations (Eqs. (34)-(37)) and boundary conditions (Eqs. (44)-(49)), all boundary conditions are satisfied and the governing equations will be presented in a matrix form as below:

$$\begin{bmatrix} S_{11} & S_{12} & S_{13} & S_{14} \\ S_{21} & S_{22} & S_{23} & S_{24} \\ S_{31} & S_{32} & S_{33} & S_{34} \\ S_{41} & S_{42} & S_{43} & S_{44} \end{bmatrix} \begin{Bmatrix} U_1 \\ V_1 \\ W_1 \\ \varphi_1 \end{Bmatrix} = \begin{Bmatrix} 0 \\ 0 \\ 0 \\ 0 \end{Bmatrix}. \tag{52}$$

The components of matrix **S** are represented in Appendix A.2 in order to investigate the critical axial buckling load.

Therefore, the determinant of the coefficients matrix must be set to zero in order to determine the non-trivial solution of Eq. (52).

It should be noted that since the current study examines the buckling of cylindrical nanoshell under the axial compression the movable boundary conditions are considered ($U_1\big|_{x=0,L} \neq 0$); therefore, the effects of temperature and electric voltage on the buckling of cylindrical nanoshell can only be considered in appropriate values of axial compression which is taken into consideration as well.

5. Results

As the first step, the results are compared with those reported in the literature to show the accuracy of the current work. Then, some numerical results are provided to indicate the usability of the derived equilibrium equations on the basis of modified couple stress theory in order to calculate the buckling behavior of piezoelectric cylindrical nanoshells subjected to thermo-electro-mechanical loads. Thus, the influences of different parameters such as dimensionless length scale parameter, h/l, length to radius ratio, L/R, the ratio of shell thickness to radius, h/R, temperature change, ΔT, the variation of Winkler-Pasternak stiffness, k_w and k_g, and external electric voltage, V_0, on the critical buckling load are represented. The cylindrical nanoshell is assumed to be made of PZT-4 with the material properties listed in Table 1 [30, 31].

It should be noted that the coefficients of thermal expansion are negative at low temperature and are positive in high temperature [9, 10]. Unless otherwise stated, the temperature change at high temperature is assumed to be $\Delta T = 50$ (K) and V_0 is assumed to be zero [9, 10]. Moreover, due to lacking experiments and molecular dynamic simulation results on the length scale parameter of modified couple stress for piezoelectric nanoshell, the dimensionless length scale parameter, l/h, is considered only theoretically in the interval of 0 to 5 in numerical examples proposed here and radius is assumed to be 2 nm.

5.1 Comparison of results

It should be noted that, this paper, for the first time, has been examined the buckling of nanoshell based on the modified couple stress theory using shell model under the thermo-electro-mechanical loads; thus, up to now, the thermo-electro-mechanical buckling of piezoelectric nanoshell is not investigated in the literature. Therefore, as mentioned before, by setting length scale parameter to zero ($l = 0$) the equilibrium equations and boundary conditions can be reduced to the classical continuum theory; thus, the accuracy of the obtained results are examined based on the classical continuum theory, which is neglected the piezoelectric effect as well. By way of comparison, according to Table 2, as it can be seen, the classical Continuum theory (CT) gives the critical buckling load in good agreement with the results, obtaining from both numerical and analytical methods, in Ref. [61]. Moreover, as it is indicated, the results obtained based on the Modified couple stress theory (MCST) are higher than those achieved through classical continuum theory. For the validation of the results in the new non-classical shell formulation, the axial buckling load obtained from Molecular mechanic (MM) simulation in Refs. [76, 77] are compared with the ones of this paper in Table 3. As it is shown, the results of MM simulation have a good accordance with the results of modified couple stress theory than classical theory in different $L/2R$'s ratios. In other words, as is determined from Table 3 the classical continuum theory results has maximum error 77.3 % compared to the results of MM simulation but by taking the value of a length scale parameter between 0.066-0.099 nm, the maximum error between the couple stress theory results and the results of MM

Table 1. Material properties of PZT-4.

c_{11} (GPa)	c_{12} (GPa)	c_{13} (GPa)	c_{33} (GPa)	c_{66} (GPa)
132	71	73	115	30.5
e_{31} (C/m^2)	e_{15} (C/m^2)	e_{33} (C/m^2)	s_{11} (C/Vm)	s_{33} (C/Vm)
-4.1	10.5	14.1	5.841e-9	7.124e-9
β_1 (N/m^{2}K)	β_3 (N/m^{2}K)	p_1 (C/m^{2}K)	p_3 (C/m^{2}K)	
4.738e5	4.529e5	0.25e-4	0.25e-4	

Table 2. Comparison of dimensionless critical buckling load wi-th different thickness.

$2R/h$	Numerical analysis [61]	Analytical analysis [61]	Present ($l = 0$)	MCST ($l = h$)
800	1.5013	1.5141	1.5131	3.4099
900	1.3586	1.3459	1.3450	3.0464
1000	1.2111	1.2113	1.2105	2.7497
1100	1.1021	1.1012	1.1005	2.4842
1200	1.0170	1.0094	1.0087	2.2783
1300	0.9365	0.9318	0.9311	2.1164
1400	0.8654	0.8652	0.8646	1.9674
1500	0.8075	0.8075	0.8069	1.8309

Table 3. The comparison of critical buckling load with the results of MM simulation in different $L/2R$ ratios.

$L/2R$	Ref. [76]	Present study	Error (%)	Present study	Error (%)
2.41	39.12	39.23 ($l = 0.096$)	0.28	22.18 ($l = 0$)	76.3
3.63	26.37	26.44 ($l = 0.079$)	0.26	21.92 ($l = 0$)	20.3
$L/2R$	Ref. [77]	Present study	Error (%)	Present study	Error (%)
2.45	39.28	39.33 ($l = 0.099$)	0.12	22.15 ($l = 0$)	77.3
3.79	27.02	27.39 ($l = 0.099$)	1.3	21.87 ($l = 0$)	23.5
4.20	22.93	23.81 ($l = 0.066$)	3.8	21.90 ($l = 0$)	4.7

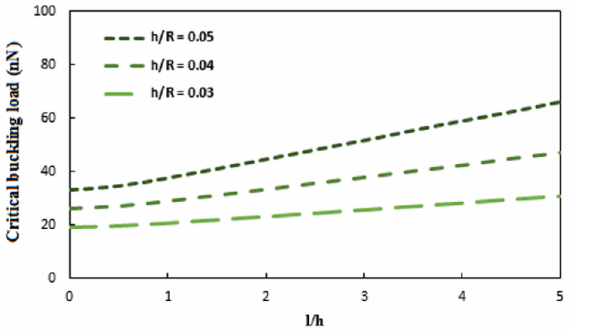

(a)

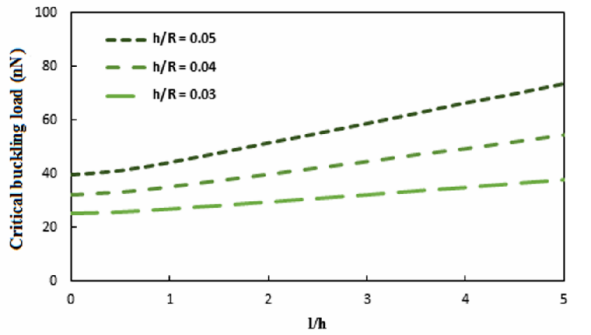

(b)

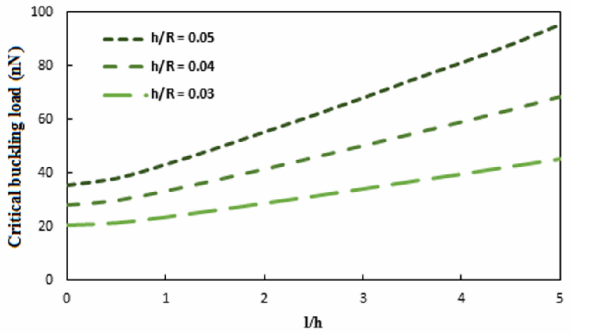

(c)

Fig. 2. The effect of dimensionless length scale parameter, h/R and elastic foundation stiffness on critical buckling load in the case of high temperature, (a) (k_w, k_g) = (0,0); (b) (k_w, k_g) = (0.5,0); (c) (k_w, k_g) = (0,10e18).

simulation are 3.8 %. Thus, the axial buckling load provided by the present size-dependent shell model are very close to the MM values.

The value of length-scale parameters is selected as $0.066 < l < 0.099$ nm to produce the best fit with the MM results. Interestingly, this model is able to accurately predict the axial buckling load of CNTs. It can be concluded that the present size-dependent model might bridge the gap between MM results and previous classic theoretical models.

5.2 Effects of dimensionless length scale parameter, thickness and elastic foundation on critical buckling load

Figs. 2(a)-(c) illustrate the influence of dimensionless length scale parameter (l/h) on critical buckling load of piezoelectric cylindrical nanoshell for three different thickness ratios (h/R) in (k_w, k_g) = (0,0), (k_w, k_g) = (0.5,0), (k_w, k_g) = (0,10e18), respectively based on the Modified couple stress theory (MCST) at high temperature. As it can be seen, by increasing dimensionless length scale parameter (l/h) due to increasing nanoshell stiffness, the critical buckling load increases on the basis of the modified couple stress theory. On the other hand, for fixed values of l/h, as h/R increases, the critical buckling load, predicted by the modified couple stress theory increases. It is also visible that, due to increase in thickness ratio h/R, the increase of critical buckling load is intensified by increasing dimensionless length scale parameter. Moreover, it is clear that, the critical buckling load presented by modified couple stress theory is greater than that of classical continuum theory (l/h = 0). Besides, the influence of Winkler and Pasternak constants on increasing the critical buckling load is proposed as well. For instance, in l/h = 1 and h/R = 0.05, by increasing k_g from 0 to 0.5, the critical buckling load increases from 37.61 to 44.1 nN, just as k_w, which increases the critical buckling load from 37.61 to 43.34 nN, when increases from 0 to 10e18.

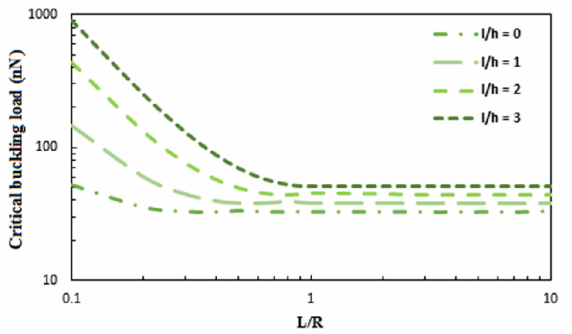

Fig. 3. The effect of length to radius ratio on critical buckling load in different l/h, in the case of high temperature.

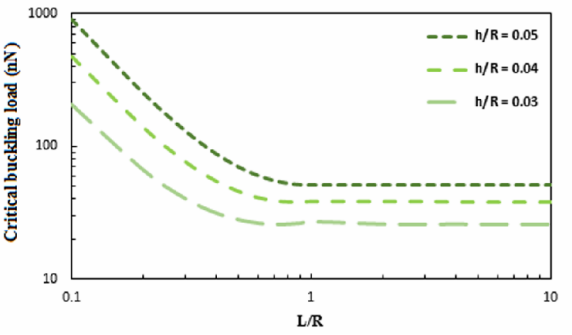

Fig. 4. The effect of length to radius ratio on critical buckling load in different h/R, in the case of high temperature.

5.3 Effects of length to radius ratio on critical buckling load

Figs. 3 and 4 indicate the effect of length to radius ratio L/R, besides l/h and h/R on critical buckling load based on the

Table 4. The influence of temperature change on the critical buckling load (nN).

	T	$L/R = 0.1$			$L/R = 1$		
		h/R			h/R		
		0.03	0.04	0.05	0.03	0.04	0.05
$l/h = 1$	-100	43.191	83.804	146.88	20.789	28.834	37.836
	-50	43.184	83.794	146.87	20.782	28.825	37.824
	0	43.177	83.785	146.86	20.774	28.815	37.812
	50	43.170	83.776	146.85	20.767	28.805	37.800
	100	43.163	83.766	146.84	20.760	28.796	37.788
$l/h = 2$	-100	104.66	229.50	431.45	23.413	35.053	45.917
	-50	104.65	229.49	431.44	23.406	35.043	45.904
	0	104.64	229.48	431.43	23.398	35.033	45.891
	50	104.63	229.47	431.41	23.391	35.024	45.878
	100	104.62	229.46	431.40	23.384	35.014	45.865

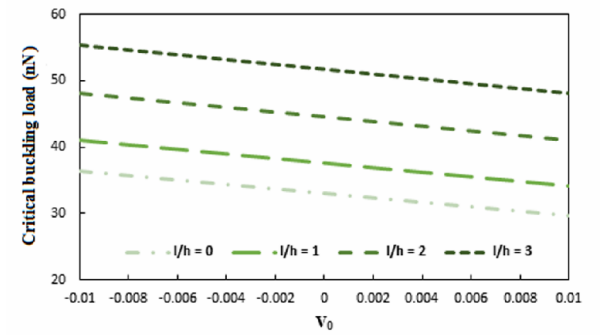

Fig. 5. Effect of external electric voltage besides l/h parameter on critical buckling load in the case of high temperature.

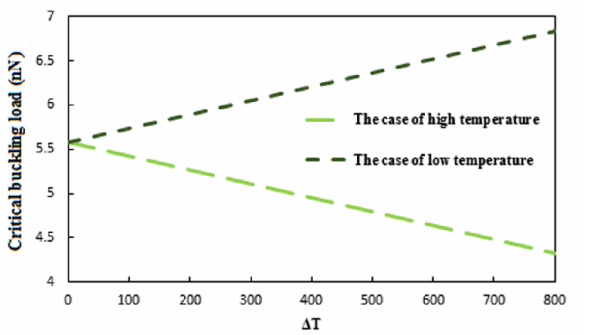

Fig. 6. Effect of temperature change on critical buckling load in the case of high and low temperature.

modified couple stress theory, respectively. In Fig. 3, as this is shown, the variations of the critical buckling load vs. the length to radius ratio on the basis of modified couple stress theory and classical continuum theory ($l/h = 0$) is similar. According to illustration, the dimensionless length scale parameter l/h intensifies the influence of length to radius ratio on the critical buckling load. Moreover, in Fig. 4, the influence of length to radius ratio L/R on critical buckling load is shown in different thickness to radius ratios, h/R, based on the modified couple stress theory ($l/h = 3$). As is visible, the influence of length to radius ratio is intensified by the increase in thickness to radius ratio, h/R.

5.4 Effects of external electric voltage on critical buckling load

Fig. 5 depicts the influence of external electric voltage on the critical buckling load besides the dimensionless length scale parameter, l/h. As it is shown, the critical buckling load decreases by increase in external electric voltage from -0.01 to 0.01. This is because of the axial compressive and tensile forces, which are generated by applying positive and negative voltages, respectively. Clearly, the negative voltage causes the higher critical buckling load. Moreover, according to Fig. 5, as increase in l/h parameter intensifies the effect of applied electric voltage on critical buckling load of piezoelectric nanoshell, the increase in dimensionless length scale par- ameter leads to higher critical buckling load with negative voltage.

5.5 Effects of temperature change on critical buckling load

The effect of temperature change ΔT at two cases of low temperature and high temperature on the critical buckling load based on the modified couple stress theory is illustrated in Fig. 6. The results indicate that, in the case of high temperature, the increase in ΔT leads to decrease in critical buckling load, due to decreasing stiffness with increasing temperature change, while the critical buckling load increases as ΔT is increased at the case of low temperature. The similar trend of the critical buckling load variation with those expressed in Refs. [10, 62] indicates the accuracy of this work.

5.6 Critical buckling load variation with regard to the different temperature and external electric voltage change

To study the effects of tempearture and external electric

Table 5. The effect of external electric voltage variation on the critical buckling load (nN).

	V_0	$L/R = 0.1$			$L/R = 1$		
		h/R			h/R		
		0.03	0.04	0.05	0.03	0.04	0.05
$l/h = 1$	-0.01	46.460	87.068	150.14	24.137	32.178	41.175
	-0.005	44.819	85.427	148.50	22.456	30.496	39.493
	0	43.177	83.785	146.86	20.774	28.815	37.812
	0.005	41.535	82.143	145.22	19.093	27.133	36.130
	0.01	39.894	80.502	143.58	17.411	25.452	34.449
$l/h = 2$	-0.01	107.92	232.76	434.71	26.761	38.396	49.503
	-0.005	106.28	231.12	433.06	25.080	36.715	47.697
	0	104.64	229.48	431.42	23.398	35.033	45.891
	0.005	103.00	227.84	429.78	21.717	33.352	44.085
	0.01	101.36	226.19	428.14	20.035	31.670	42.279

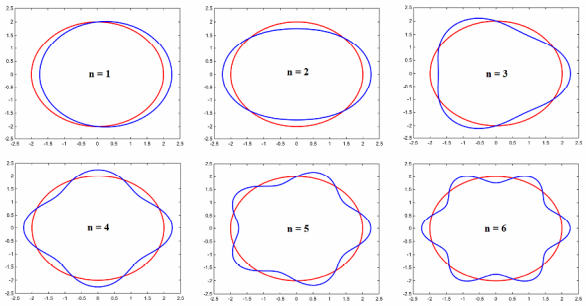

Fig. 7. Buckling mode shapes of cylindrical nanoshell.

voltage change on the buckling response of piezoelectric cylindrical nanoshell, the variation of critical buckling load with respect to the thickness and length ratio for different dimensionless length scale parameter are illustrated in Tables 4 and 5. As it can be seen from these tables, the critical buckling load is significantly size dependent; such that, increase in material length scale parameter increases the critical buckling load in different temperature and external electric voltage. Besides, increase in thickness ratio and decrease in length ratio which increases the critical buckling load is visible at all temperature and external electric voltage too. Consequently, however increase in temperature and external electric voltage decreases the critical buckling load, the variation of critical buckling load is similar in different temperature and external electric voltage for different thickness and length ratio and dimensionless length scale parameters. Moreover, the buckling modes for n = 1-6 are represented in Fig. 7.

6. Conclusion

In this article, the buckling behavior of a geometrically nonlinear cylindrical nanoshell resting on Winkler-Pasternak foundation was examined on the basis of the modified couple stress theory and shell model, subjected to an axial compression, an applied voltage and uniform temperature change.

The size effect was considered using the modified couple stress theory. The minimum potential energy principle was utilized to derive the equilibrium equations and boundary conditions.

Ultimately, using the Navier solution, the buckling of a nanoshell with simply supported boundary conditions was investigated and the effects of different parameters such as dimensionless length scale parameter, length and thickness to radius ratio, temperature change, Winkler and Pasternak stiffness and external electric voltage on critical buckling load was examined based on the modified couple stress theory and the classical continuum theory, by setting $l = 0$.

Thus, it is indicated that, the increase in dimensionless length scale parameter leads to increasing the critical buckling load and even intensifying the influence of other parameters, such as applied voltage, on the critical buckling load.

Nomenclature

σ_{ij} : Cauchy stress tensor
D_i : Electric displacement vector
m_{ij} : Higher order stress tensor
ε_{ij} : Strain tensor
E_i : Electric field vector
χ_{ij} : Symmetric part of rotation gradient tensor
c_{ijkl} : Elastic tensor
e_{mij} : Piezoelectric constants
s_{im} : Dielectric constants
β_{ij} : Thermal moduli
p_i : Pyroelectric constants
u_i : Displacement vector
φ : Electric potential
ΔT : Temperature change
l : Material length scale parameter
e_{ipq} : Permutation symbol
η_{ipq} : Deviatoric stretch gradient tensor
$\tilde{c}_{ij}$: Reduced elastic constants

$\tilde{e}_{ij}$: Reduced piezoelectric constants
$\tilde{s}_{ij}$: Reduced dielectric constants
$\tilde{\beta}_i$: Reduced thermal moduli
$\tilde{p}_i$: Reduced pyroelectric constants
V_0 : External electric voltage
$\delta\tilde{U}_s$: Strain energy variation
$\delta\tilde{W}$: Variation of the work of external forces
P : External axial compression load
k_w : Winkler foundation stiffness
k_g : Shear subgrade modulus of the foundation
U_0, V_0, W_0 : Displacement components of the equilibrium state
U_1, V_1, W_1 : Arbitrary small increment

References

[1] Z. W. Pan, Z. R. Dai and Z. L. Wang, Nanobelts of semiconducting oxides, *Science,* 291 (5510) (2001) 1947-1949.

[2] P. Fei et al., Piezoelectric potential gated field-effect transistor based on a free-standing ZnO wire, *Nano Letters*, 9 (10) (2009) 3435-3439.

[3] Z. L. Wang and J. Song, Piezoelectric nanogenerators based on zinc oxide nanowire arrays, *Science,* 312 (5771) (2006) 242-246.

[4] J. H. He et al., Piezoelectric gated diode of a single ZnO nanowire, *Advanced Materials*, 19 (6) (2007) 781-784.

[5] A. Alibeigloo and A. M. Kani, 3D free vibration analysis of laminated cylindrical shell integrated piezoelectric layers using the differential quadrature method, *Applied Mathematical Modelling*, 34 (12) (2010) 4123-4137.

[6] G. G. Sheng and X. Wang, Active control of functionally graded laminated cylindrical shells, *Composite Structures*, 90 (4) (2009) 448-457.

[7] A. T. Samaei, M. Bakhtiari and G. F. Wang, Timoshenko beam model for buckling of piezoelectric nanowires with surface effects, *Nanoscale Research Letters*, 7 (1) (2012) 1-6.

[8] Z. Yan and L. Y. Jiang, Vibration and buckling analysis of a piezoelectric nanoplate considering surface effects and in-plane constraints, *Proceedings of the Royal Society of London A: Mathematical, Physical and Engineering Sciences*, The Royal Society (2012).

[9] A. G. Arani et al., Electro-thermo-torsional buckling of an embedded armchair DWBNNT using nonlocal shear deformable shell model, *Composites Part B: Engineering*, 51 (2013) 291-299.

[10] A. G. Arani et al., Electro-thermo-mechanical buckling of DWBNNTs embedded in bundle of CNTs using nonlocal piezoelasticity cylindrical shell theory, *Composites Part B: Engineering*, 43 (2) (2012) 195-203.

[11] R. Chowdhury et al., A molecular mechanics approach for the vibration of single-walled carbon nanotubes, *Computational Materials Science*, 48 (4) (2010) 730-735.

[12] R. Chowdhury, S. Adhikari and F. Scarpa, Vibration of ZnO nanotubes: A molecular mechanics approach, *Applied Physics A*, 102 (2) (2011) 301-308.

[13] Y. Xiaohu and Q. Han, The thermal effect on axially compressed buckling of a double-walled carbon nanotube, *European Journal of Mechanics-A/Solids,* 26 (2) (2007) 298-312.

[14] K. M. Liew and Q. Wang, Analysis of wave propagation in carbon nanotubes via elastic shell theories, *International Journal of Engineering Science*, 45 (2) (2007) 227-241.

[15] R. Ansari and M. Hemmatnezhad, Nonlinear vibrations of embedded multi-walled carbon nanotubes using a variational approach, *Mathematical and Computer Modelling*, 53 (5) (2011) 927-938.

[16] Q. Ma and D. R. Clarke, Size dependent hardness of silver single crystals, *Journal of Materials Research*, 10 (4) (1995) 853-863.

[17] J. S. Stölken and A. G. Evans, A microbend test method for measuring the plasticity length scale, *Acta Materialia,* 46 (14) (1998) 5109-5115.

[18] M. Mohammad-Abadi and A. R. Daneshmehr, Size dependent buckling analysis of microbeams based on modified couple stress theory with high order theories and general boundary conditions, *International Journal of Engineering Science*, 74 (2014) 1-14.

[19] P. Mohammadi Dashtaki and Y. Tadi Beni, Effects of Casimir force and thermal stresses on the buckling of electrostatic nano-bridges based on couple stress theory, *Arabian Journal for Science and Engineering*, 39 (2014) 5753-5763.

[20] M. Shojaeian, Y. Tadi Beni and H. Ataei, Size-dependent snap-through and pull-in instabilities of initially curved pre-stressed electrostatic nano-bridges, *Journal of Physics D: Applied Physics*, 49 (2016) 295303.

[21] F. Kheibari and Y. Tadi Beni, Size dependent electromechanical vibration of single-walled piezoelectric nanotubes using thin shell model, *Materials & Design*, 114 (2017) 572-583.

[22] H. Razavi, A. Faramarzi Babadi and Y. Tadi Beni, Free vibration analysis of functionally graded piezoelectric cylindrical nanoshell based on consistent couple stress theory, *Composite Structures*, 160 (2017) 1299-1309.

[23] Y. Tadi Beni, M. R. Abadyan and A. R. Noghrehabadi, Investigation of size effect on the pull-in instability of beam type NEMS under van der Waals attraction, *Procedia Engineering*, 10 (2011) 1718-1723.

[24] Y. Tadi Beni, A. Koochi and M. R. Abadyan, Using modified couple stress theory for modeling the size dependent pull-in instability of torsional nano-mirror under Casimir force, *International Journal of Optomechatronics*, 8 (2014) 47-71.

[25] Y. Tadi Beni, A nonlinear electro-mechanical analysis of nanobeams based on the size-dependent piezoelectricity theory, *Journal of Mechanics*, 65 (2016a) 1-13.

[26] Y. Tadi Beni, Size-dependent electromechanical bending, buckling, and free vibration analysis of functionally graded piezoelectric nanobeams, *Journal of Intelligent Material Systems and Structures*, 27 (2016b) 2199-2215.

[27] Y. Tadi Beni, Size-dependent analysis of piezoelectric nanobeams including electro-mechanical coupling, *Mechanics Research Communications*, 75 (2016c) 67-80.

[28] A. C. Eringen, Nonlocal polar elastic conti ua, *International Journal of Engineering Science,* 10 (1) (1972) 1-16.
[29] A. C. Eringen, *Nonlocal polar field models*, Academic, New York (1976).
[30] C. Liu et al., Thermo-electro-mechanical vibration of piezoelectric nanoplates based on the nonlocal theory, *Composite Structures*, 106 (2013) 167-174.
[31] L. L. Ke, Y. S. Wang and J. N. Reddy, Thermo-electro-mechanical vibration of size-dependent piezoelectric cylindrical nanoshells under various boundary conditions, *Composite Structures*, 116 (2014) 626-636.
[32] R. D. Mindlin, Micro-structure in linear elasticity, *Archive for Rational Mechanics and Analysis*, 16 (1) (1964) 51-78.
[33] R. A. Toupin, Elastic materials with couple-stresses, *Archive for Rational Mechanics and Analysis*, 11 (1) (1962) 385-414.
[34] W. T. Koiter, *Couple-stresses in the theory of elasticity*, I & II (1969) 17-44.
[35] S. J. Zhou and Z. Q. Li, Length scales in the static and dynamic torsion of a circular cylindrical micro-bar, *Journal of Shandong University of Technology* (2001) 401-407.
[36] X. Kang and W. X. XI, Size effect on the dynamic characteristic of a micro beam based on Cosserat theory, *Journal of Engineering Strength* (2007) 1-4.
[37] F. Yang et al., Couple stress based strain gradient theory for elasticity, *International Journal of Solids and Structures*, 39 (10) (2002) 2731-2743.
[38] S. Sahmani et al., Dynamic stability analysis of functionally graded higher-order shear deformable microshells based on the modified couple stress elasticity theory, *Composites Part B: Engineering*, 51 (2013) 44-53.
[39] J. Kim and J. N. Reddy, Analytical solutions for bending, vibration, and buckling of FGM plates using a couple stress-based third-order theory, *Composite Structures*, 103 (2013) 86-98.
[40] R. D. Mindlin, Micro-structure in linear elasticity, *Archive for Rational Mechanics and Analysis,* 16 (1) (1964) 51-78.
[41] R. D. Mindlin, Second gradient of strain and surface-tension in linear elasticity, *International Journal of Solids and Structures*, 1 (4) (1965) 417-438.
[42] N. A. Fleck and J. W. Hutchinson, Strain gradient plasticity, *Advances in Applied Mechanics*, 33 (1997) 296-361.
[43] D. C. C. Lam et al., Experiments and theory in strain gradient elasticity, *Journal of the Mechanics and Physics of Solids*, 51 (8) (2003) 1477-1508.
[44] R. Gholami et al., Size-dependent axial buckling analysis of functionally graded circular cylindrical microshells based on the modified strain gradient elasticity theory, *Meccanica*, 49 (7) (2014) 1679-1695.
[45] B. Akgöz and Ö. Civalek, A new trigonometric beam model for buckling of strain gradient microbeams, *International Journal of Mechanical Sciences*, 81 (2014) 88-94.
[46] F. Mehralian, Y. Tadi Beni and R. Ansari, On the size dependent buckling of anisotropic piezoelectric cylindrical shells under combined axial compression and lateral pressure, *International Journal of Mechanical Sciences,* 119 (2016) 155-169.
[47] S. Sahmani, M. M. Aghdam and M. Bahrami, On the post-buckling behavior of geometrically imperfect cylindrical nanoshells subjected to radial compression including surface stress effects, *Composite Structures* (2015).
[48] A. Baninajjaryan and Y. Tadi Beni, Theoretical study of the effect of shear deformable shell model, elastic foundation and size dependency on the vibration of protein microtubule, *Journal of Theoretical Biology*, 382 (2015) 111-121.
[49] H. Zeighampour, Y. Tadi Beni and F. Mehralian, A shear deformable conical shell formulation in the framework of couple stress theory, *Acta Mechanica* (2015) 1-23.
[50] F. Mehralian and Y. Tadi Beni, Size-dependent torsional buckling analysis of functionally graded cylindrical shell, *Composites Part B: Engineering,* 94 (2016) 11-25.
[51] R. Ansari et al., Size-dependent vibration and instability of fluid-conveying functionally graded microshells based on the modified couple stress theory, *Microfluidics and Nanofluidics* (2015) 1-14.
[52] Y. Tadi Beni, F. Mehralian and H. Razavi, Free vibration analysis of size-dependent shear deformable functionally graded cylindrical shell on the basis of modified couple stress theory, *Composite Structures*, 120 (2015) 65-78.
[53] A. Alibeigloo and M. Shaban, Free vibration analysis of carbon nanotubes by using three-dimensional theory of elasticity, *Acta Mechanica*, 224 (7) (2013) 1415-1427.
[54] M. K. Zeverdejani and Y. Tadi Beni, The nano scale vibration of protein microtubules based on modified strain gradient theory, *Current Applied Physics*, 13 (8) (2013) 1566-1576.
[55] Q. Wang, On buckling of column structures with a pair of piezoelectric layers, *Engineering Structures*, 24 (2) (2002) 199-205.
[56] A. W. Leissa, *Vibration of shells*, Washington, DC, USA: Scientific and Technical Information Office, National Aeronautics and Space Administration, 288 (1973).
[57] K. Dong and X. Wang, Wave propagation characteristics in piezoelectric cylindrical laminated shells under large deformation, *Composite Structures*, 77 (2) (2007) 171-181.
[58] D. O. Brush and B. O. Almroth, *Buckling of Bars, Plates, and Shells* (1979).
[59] S. R. Asemi and A. Farajpour, Thermo-electro-mechanical vibration of coupled piezoelectric-nanoplate systems under non-uniform voltage distribution embedded in Pasternak elastic medium, *Current Applied Physics*, 14 (5) (2014) 814-832.
[60] T. Murmu and S. C. Pradhan, Thermo-mechanical vibration of a single-walled carbon nanotube embedded in an elastic medium based on nonlocal elasticity theory, *Computational Materials Science*, 46 (4) (2009) 854-859.
[61] S. E. Kim and C. S. Kim, Buckling strength of the cylindrical shell and tank subjected to axially compressive loads, *Thin-walled Structures*, 40 (4) (2002) 329-353.
[62] M. J. Hao, X. M. Guo and Q. Wang, Small-scale effect on

torsional buckling of multi-walled carbon nanotubes, *European Journal of Mechanics-A/Solids*, 29 (1) (2010) 49-55.

[63] L. L. Ke, Y. S. Wang, J. Yang and S. Kitipornchai, Free vibration of size-dependent magneto-electro-elastic nanoplates based on the nonlocal theory, *Acta Mechanica Sinica,* 30 (4) (2014) 516-525.

[64] Y. S. Li, W. J. Feng and Z. Y. Cai, Bending and free vibration of functionally graded piezoelectric beam based on modified strain gradient theory, *Composite Structures,* 115 (2014) 41-50.

[65] Y. S. Li and E. Pan, Static bending and free vibration of a functionally graded piezoelectric microplate based on the modified couple-stress theory, *International Journal of Engineering Science,* 97 (2015) 40-59.

[66] L. L. Ke, Y. S. Wang, J. Yang and S. Kitipornchai, The size-dependent vibration of embedded magneto-electro-elastic cylindrical nanoshells, *Smart Materials and Structures,* 23 (12) (2014) 125036.

[67] F. Ebrahimi and E. Salari, Size-dependent thermo-electrical buckling analysis of functionally graded piezoelectric nanobeams, *Smart Materials and Structures,* 24 (12) (2015) 125007.

[68] Y. S. Li and E. Pan, Bending of a sinusoidal piezoelectric nanoplate with surface effect, *Composite Structures,* 136 (2016) 45-55.

[69] A. Ghorbanpour Arani, S. A. Mortazavi, R. Kolahchi and AH. Ghorbanpour Arani, Vibration response of an elastically connected double-smart nanobeam-system based nano-electro-mechanical sensor, *Journal of Solid Mechanics,* 7 (2) (2015) 121-130.

[70] A. A. Jandaghian and O. Rahmani, Free vibration analysis of magneto-electro-thermo-elastic nanobeams resting on a Pasternak foundation, *Smart Materials and Structures,* 25 (3) (2016) 035023.

[71] R. Ansari and R. Gholami, Size-dependent buckling and postbuckling analyses of first-order shear deformable magneto-electro-thermo elastic nanoplates based on the nonlocal elasticity theory, *International Journal of Structural Stability and Dynamics* (2016) 1750014.

[72] A. Ghorbanpour Arani, M. Jamali, M. Mosayyebi and R. Kolahchi, Wave propagation in FG-CNT-reinforced piezoelectric composite micro plates using viscoelastic quasi-3D sinusoidal shear deformation theory, *Composites Part B: Engineering,* 95 (2016) 209-224.

[73] A. A. Jandaghian and O. Rahmani, An analytical solution for free vibration of piezoelectric nanobeams based on a nonlocal elasticity theory, *Journal of Mechanics,* 32 (2) (2016) 143-151.

[74] R. Ansari, M. Faraji Oskouie, R. Gholami and F. Sadeghi, Thermo-electro-mechanical vibration of postbuckled piezoelectric Timoshenko nanobeams based on the nonlocal elasticity theory, *Composites Part B: Engineering,* 89 (2016) 316-327.

[75] F. Ebrahimi and M. R. Barati, Electromechanical buckling behavior of smart piezoelectrically actuated higher-order size-dependent graded nanoscale beams in thermal environment, *International Journal of Smart and Nano Materials,* 7 (2) (2016) 69-90.

[76] G. I. Giannopoulos, A. P. Tsiros and S. K. Georgantzinos, Prediction of elastic mechanical behavior and stability of single-walled carbon nanotubes using bar elements, *Mechanics of Advanced Materials and Structures,* 20 (9) (2013) 730-741.

[77] N. Hu, K. Nunoya, D. Pan, T. Okabe and H. Fukunaga, Prediction of buckling characteristics of carbon nanotubes, *International Journal of Solids and Structures,* 44 (2007) 6535-6550.

[78] X. H. Yao and Y. Sun, Combined bending stability of carbon nanotubes subjected to thermo-electro-mechanical loadings, *Computational Materials Science,* 54 (2012) 135-144.

[79] X. H. Yao, Y. G. Sun and H. Z. Li, Combined torsional buckling of carbon nanotubes subjected to thermo-electro-mechanical loadings with consideration of scale effect, *Key Engineering Materials,* Trans Tech. Publications, 562 (2013) 744-749.

[80] F. Ebrahimi and M. R. Barati, Temperature distribution effects on buckling behavior of smart heterogeneous nanosize plates based on nonlocal four-variable refined plate theory, *International Journal of Smart and Nano Materials,* 7 (3) (2016) 119-143.

[81] E. Bagherizadeh, Y. Kiani and M. R. Eslami, Mechanical buckling of functionally graded material cylindrical shells surrounded by Pasternak elastic foundation, *Composite Structures,* 93 (11) (2011) 3063-3071.

[82] G. G. Sheng and X. Wang, Thermoelastic vibration and buckling analysis of functionally graded piezoelectric cylindrical shells, *Applied Mathematical Modelling,* 34 (9) (2010) 2630-2643.

Appendix

A.1

The constant coefficient A_1 to A_9, B_1 to B_{10} and C_1 to C_{13} in Eqs. (21)-(24) are obtained as below:

$$A_1 = -\tilde{c}_{11}\,\mathrm{h},\ A_2 = \frac{\tilde{c}_{66}hl^2}{4R^2},\ A_3 = -\frac{\tilde{c}_{66}hl^2}{4R}, \tag{A.1}$$

$$A_4 = -\frac{\tilde{c}_{12}h}{R} - \frac{\tilde{c}_{66}h}{R},\ A_5 = -\frac{\tilde{c}_{66}hl^2}{4R^3},\ A_6 = -\frac{\tilde{c}_{12}h}{R},$$

$$A_7 = -\frac{3\tilde{c}_{66}hl^2}{2R^3}, A_8 = -\frac{\tilde{c}_{66}h}{R^2}\left(1+\frac{l^2}{R^2}\right), A_9 = \frac{\tilde{c}_{66}hl^2}{4R^4},$$

$$B_1 = \frac{\tilde{c}_{66}hl^2}{4},\ B_2 = -\tilde{c}_{66}h\left(1+\frac{3l^2}{R^2}\right), B_3 = -\frac{\tilde{c}_{11}h}{R^2} - \frac{\tilde{c}_{66}hl^2}{R^4},$$

$$B_4 = \frac{\tilde{c}_{66}hl^2}{4R^2},\ B_5 = -\frac{\tilde{c}_{66}hl^2}{4R}, B_6 = -\frac{\tilde{c}_{66}hl^2}{4R^3}, B_7 = -\frac{\tilde{c}_{12}h}{R} - \frac{\tilde{c}_{66}h}{R},$$

$$B_8 = \frac{5\tilde{c}_{66}hl^2}{2R^2}, B_9 = \frac{\tilde{c}_{66}hl^2}{R^4}, B_{10} = -\frac{\tilde{c}_{11}h}{R^2},$$

$$C_1 = \frac{\tilde{c}_{11}h^3}{12} + \tilde{c}_{66}hl^2,\ C_2 = -\frac{\tilde{c}_{66}hl^2}{R^2},$$

$$C_3=\frac{\tilde{c}_{12}h^3}{6R^2}+\frac{\tilde{c}_{66}h^3}{R^2}\left(\frac{1}{3}+\frac{l^2}{12R^2}\right)+\frac{2\tilde{c}_{66}hl^2}{R^2},$$
$$C_4=\frac{\tilde{c}_{12}h}{R},C_5=\frac{3\tilde{c}_{66}hl^2}{2R^3},\ C_6=-\frac{5\tilde{c}_{66}hl^2}{2R^2},C_7=\frac{\tilde{c}_{11}h}{R^2},$$
$$C_8=-\frac{\tilde{c}_{66}hl^2}{R^4},\ C_9=\frac{\tilde{c}_{11}h}{R^2},\ C_{10}=\frac{\tilde{c}_{11}h^3}{12R^4}+\frac{\tilde{c}_{66}hl^2}{R^4},$$
$$C_{11}=-\frac{2\tilde{e}_{31}h}{\pi},C_{12}=-\frac{2\tilde{e}_{31}h}{\pi R^2},\ C_{13}=\frac{2\tilde{e}_{31}V_0}{R}-\frac{\tilde{\beta}_1\Delta Th}{R}$$
$$D_1=\frac{\tilde{s}_{11}h}{2},\ D_2=\frac{\tilde{s}_{11}h}{2R^2},\ D_3=-\frac{2\tilde{e}_{31}h}{\pi},$$
$$D_4=-\frac{2\tilde{e}_{31}h}{\pi R^2},\ D_5=-\frac{\tilde{s}_{33}\pi^2}{2h}$$

The constant coefficients a_1 to a_6, b_1 to b_9 and c_1 to c_{10} in Eqs. (26)-(31) are achieved as:

$$a_1=\tilde{c}_{11}h,\ a_2=-\frac{\tilde{c}_{66}hl^2}{4R^2},a_3=\frac{\tilde{c}_{66}hl^2}{4R},a_4=\frac{\tilde{c}_{12}h}{R},$$
$$a_5=\frac{\tilde{c}_{12}h}{R},\ \mathrm{c}_6=-\frac{P}{2\pi R}+2\tilde{e}_{31}\mathrm{V}_0-\tilde{\beta}_1\Delta\mathrm{Th} \quad \text{(A.2)}$$
$$b_1=-\frac{\tilde{c}_{66}hl^2}{4},b_2=\tilde{c}_{66}h\left(1+\frac{3l^2}{R^2}\right),b_3=-\frac{\tilde{c}_{66}hl^2}{4R^2},b_4=\frac{\tilde{c}_{66}hl^2}{4R},$$
$$b_5=\frac{\tilde{c}_{66}hl^2}{4R^3},\ b_6=\frac{\tilde{c}_{66}h}{R},b_7=-\frac{7\tilde{c}_{66}hl^2}{2R^2},b_8=-\frac{\tilde{c}_{66}hl^2}{4R},$$
$$b_9=\frac{\tilde{c}_{66}hl^2}{4},\ c_1=-\frac{\tilde{c}_{11}h^3}{12}-\tilde{c}_{66}hl^2,c_2=\frac{\tilde{c}_{66}hl^2}{R^2},$$
$$c_3=-\frac{\tilde{c}_{12}h^3}{12R^2}-\frac{\tilde{c}_{66}h^3}{3R^2}-\frac{\tilde{c}_{66}h^3l^2}{6R^4}-\frac{3\tilde{c}_{66}hl^2}{R^2},$$
$$c_4=-\frac{3\tilde{c}_{66}hl^2}{2R^3},\ c_5=\frac{5\tilde{c}_{66}hl^2}{2R^2},\ c_6=-\frac{2\tilde{e}_{31}h}{\pi},$$
$$c_7=\frac{\tilde{c}_{11}h^3}{12}+\tilde{c}_{66}hl^2,c_8=\frac{\tilde{c}_{12}h^3}{R^2}-\frac{\tilde{c}_{66}hl^2}{R^2},$$
$$c_9=\frac{\tilde{c}_{66}hl^2}{R^2},\ c_{10}=-\frac{2\tilde{e}_{31}h}{\pi},d_1=-\frac{\tilde{s}_{11}h}{2}.$$

A.2

The components of **S** matrix in Eq. (52) are achieved as below:

$$S_{11}=R^4\beta^4A_9+R^2\alpha^2\beta^2A_2-R^2\beta^2A_8-\alpha^2A_1 \quad \text{(A.3)}$$
$$S_{12}=-R^3\alpha\beta^3A_5-R\alpha^3\beta A_3+R\alpha\beta A_4$$
$$S_{13}=-R^2\alpha\beta^2A_7+\alpha A_6,\ \ S_{14}=0$$
$$S_{21}=-R^3\alpha\beta^3B_6-R\alpha^3\beta B_5+R\alpha\beta B_7$$
$$S_{22}=R^2\alpha^2\beta^2B_4-R^2\beta^2B_3+\alpha^4B_1-\alpha^2B_2$$
$$S_{23}=R^3\beta^3B_9+R\alpha^2\beta B_8-R\beta B_{10},\ \ S_{24}=0$$
$$S_{31}=R^2\alpha\beta^2C_5-\alpha C_4$$
$$S_{32}=-R^3\beta^3C_8-R\alpha^2\beta C_6+R\beta C_7$$
$$S_{33}=C_1\alpha^4-C_2\alpha^2+C_3R^2\beta^2\alpha^2+C_9+C_{10}R^4\beta^4$$
$$-\left(\frac{P}{2\pi R}+\tilde{\beta}_1h\Delta T-2\tilde{e}_{31}V_0\right)\alpha^2-\left(\tilde{\beta}_1h\Delta T-2\tilde{e}_{31}V_0\right)\beta^2$$
$$+k_w+k_g\left(\alpha^2+\beta^2\right)$$
$$S_{34}=-\alpha^2C_{11}-R^2\beta^2C_{12},\ \ S_{41}=0,\ \ S_{42}=0$$
$$S_{43}=-R^2\beta^2D_4-\alpha^2D_3,\ \ S_{44}=-R^2\beta^2D_2-\alpha^2D_1+D_5$$

where

$$\alpha=\frac{m\pi}{L}\text{ and }\beta=\frac{n}{R}.$$

Fahimeh Mehralian is a Ph.D. student of mechanical engineering at Shahrekord University. She received her B.Sc. and M.Sc. in mechanical engineering from Shahrekord University in 2010 and 2012, respectively. Her research interests are nano-mechanics, atomistic simulations and applied mechanics.

Yaghoub Tadi Beni is an Associated Professor of mechanical engineering at Shahrekord University. He received his B.Sc. in mechanical engineering from Isfahan University of Technology in 2000, and M.Sc. and Ph.D. in mechanical engineering from Sharif University of Technology in 2003 and 2009, respectively. His major research interests are in general areas of nano-mechanics with particular reference to computational mechanics, non-classical continuum theories, nonlinear analysis of plates and shells and modeling nano-structural stability.